RJC

RASĀYAN J. Chem.
Vol. 19 | No. 4 | 1993-2000 | October-December | 2026
ISSN: 0974-1496 | e-ISSN: 0976-0083 | CODEN: RJCABP
http://www.rasayanjournal.com
http://www.rasayanjournal.co.in

LIGHTWEIGHT AND HIGH-PERFORMANCE FIBRE-REINFORCED POLYMER COMPOSITE DRIVE SHAFTS THROUGH OPTIMIZED FIBER ORIENTATION AND LAMINATE ARCHITECTURE

D. Prakash, S. M. Vinoth✉, and B. Ravi Kumar
School of Mechanical Engineering, SASTRA Deemed to be University, Thanjavur, Tamilnadu, India, 613401.
✉Corresponding author: martinvinoth@mech.sastra.edu

ABSTRACT

Drive shafts are critical torque-transmission components in automotive systems and are conventionally manufactured from SM45C steel, whose high density increases weight and rotational inertia. This study investigates carbon and E-glass fibre-reinforced polymer (FRP) composites as lightweight alternatives using the finite element method (FEM). A validated steel drive shaft model was developed in ANSYS and compared with composite designs to evaluate the influence of fibre orientation and laminate stacking sequence on buckling torque, failure torque, and natural frequency. The optimised composite shafts exhibited superior mechanical and dynamic performance, achieving 30–40% weight reduction and enhanced vibration characteristics compared with the steel shaft. These findings demonstrate that optimised FRP composite drive shafts offer an effective solution for lightweight, energy-efficient, and high-performance automotive applications, contributing to SDG-9: Industry, Innovation and Infrastructure through advanced materials and SDG-12: Responsible Consumption and Production by improving material efficiency and reducing vehicle weight.

Keywords: FRP, Carbon Fibre, E-Glass Fibre, Fibre Orientation, Stacking Sequence, SDG-9, SDG-12.

RASĀYAN *J. Chem.*, Vol. 19, No.4, 2026

INTRODUCTION

In vehicle power transmission systems, torque is transmitted from the engine to the rear wheels through a drive shaft connected to a differential gearbox.[1] Conventionally, these shafts are manufactured from high-strength steel and are typically designed as two-piece assemblies joined by universal joints. However, steel shafts exhibit a high mass moment of inertia, which limits critical speed and adversely affects dynamic performance. To address these limitations, composite materials have been increasingly explored as an alternative. The application of composite drive shafts in automotive systems was first introduced by the Spicer U-joint division in 1985.[2] Subsequent studies, demonstrated that properly designed composite shafts can significantly reduce weight while achieving superior mechanical performance compared to steel.[3-4] The advancement in fibre-reinforced composites manufacturing, especially carbon fibre-reinforced composites (CFRP) and hybrid carbon/glass laminates, offers enhanced specific stiffness, torsional strength, and buckling resistance. These characteristics make them highly suitable for long drive shaft applications, where reduced weight and improved vibration performance are critical.[5-7] Jaen-Sola et al. explored the feasibility of employing low-density materials for rotor and stator shafts in generators, where they optimised and compared steel and composite alternatives.[8] Their findings indicated that, for rotating components, materials with a high elastic modulus-to-density ratio are most suitable, as they provide the desired combination of lightweight characteristics and adequate strength. Zhang et al. applied a multiscale reliability-based design optimisation method to carbon fibre reinforced polymer CFRP drive shafts and showed that optimised laminate configurations can reduce weight by over 30% while maintaining sufficient stability, whereas unfavourable stacking sequences significantly decreased buckling capacity and dynamic performance.[9] Halilbeşe et al. performed a comprehensive analysis on torsional vibration behaviour of shafts in marine propulsion systems using finite element analysis.[10] The authors reported that the stacking sequence significantly influenced the natural frequency and torsional angle in the shaft. In another study, Henry et al. optimised the carbon fibre composite shaft for projectile impact survivability.[11] Fibre orientation and stacking sequence in composite shafts have a significant impact on torsional stiffness, fundamental frequency, and buckling stiffness.[12-13] Lower fibre angles enhance natural frequency, while ±45° orientations offer maximum torsional stiffness and load capacity, according to finite element analysis and experimental confirmation.[14-16] Research on vehicle propeller shafts shows that hybrid aluminum-glass/epoxy composite shafts greatly reduce weight while satisfying torque and key speed criteria when used in place of traditional two-piece steel shafts.[17] Filament-wound composite layers greatly enhance bending fatigue performance, according to experimental research on hybrid aluminum/composite drive shafts. According to failure analysis, fibres mostly stay intact during fatigue, although cracks start in resin-rich areas and spread under cyclic stress.[18-19] Despite significant progress in the development of composite drive shafts, previous studies have primarily focused on individual aspects such as torsional strength, buckling behaviour, or vibration characteristics. A systematic investigation of the combined influence of fibre orientation and laminate stacking sequence on buckling torque, failure torque, and natural frequency, together with a comparative evaluation of carbon/epoxy and E-glass/epoxy composites against conventional steel shafts, remains limited. Therefore, this study employs a validated finite element approach to optimise composite drive shaft design for lightweight, high-performance, and sustainable automotive applications.

EXPERIMENTAL

Finite Element Analysis on Composite Material Drive Shaft

The composite drive shaft model was prepared as a hollow structure using ANSYS. Composite modelling involved defining fabric systems, creating rosettes, assigning oriented sets, and modelling plies. An initial pseudo-thickness of 1 mm was used for meshing, which was later replaced with the actual laminate thickness during composite preprocessing. Two material systems—carbon fiber with epoxy and E-glass fibre with epoxy—were defined with their respective properties. A parallel rosette was applied with one end as the reference origin, and oriented sets were used to define the ply lay-up directions.

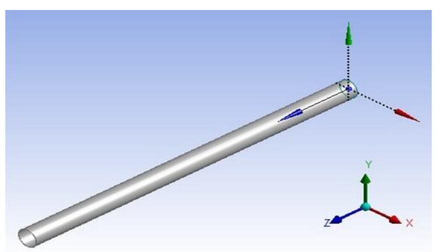

Fig.-1: Typical Geometry of Hollow Shaft in Isometric View

Since the external diameter (*Do*) of the shaft was kept constant, the composite plies were stacked inward, thereby increasing only the inner thickness as layers were added. After incorporating the required number of plies with corresponding fiber orientation angles, the solid composite shell model was generated, with epoxy resin assigned as the global drop-off material. Figure-1 shows the 3D model of the hollow shaft, and the mechanical properties are summarised in Tables-1 and 2.

Table-1: Material Properties of Carbon and E-glass Reinforced Composite Laminates

Material properties	Carbon- epoxy	E-glass-epoxy
Volume fraction V_f (%)	60	60
Longitudinal elastic modulus E_1 (GPa)	126.9	40.3
Transverse elastic modulus E_2 (GPa)	11.0	6.21
Shear modulus G_{12} (GPa)	6.6	3.07
Poisson ratio μ_{12}	0.28	0.2
Longitudinal tensile strength S_{1t} (GPa)	1.170	0.827
Density ρ (kg.m^{-3})	1610	1910
Ply thickness t_{ply} (mm)	0.635	0.1905

Table-2: Mechanical Properties of Structural Steel (SM45C)

Material Properties	Steel (SM45C)
Density ρ (kg.m^{-3})	7600
Youngs modulus E (Gpa)	207
Poisson ratio μ	0.293
Shear modulus G (Gpa)	80
Tensile yield strength σ_y (Gpa)	0.37
Ultimate tensile strength $\sigma_{rupture}$ (Gpa)	0.6

Static Structural Analysis

In this analysis, the drive shaft was subjected to a torsional load applied at one end, while the opposite end was fully constrained in all degrees of freedom (DOF). An angular displacement about the z-axis was imposed at the loaded end, and a moment reaction probe was used to measure the reaction torque at that point. This provided the torque required to produce the corresponding angular displacement.

Modal Analysis

In the analysis, the natural frequencies of the drive shaft were determined without applying any external loads. The shaft was modelled as simply supported at both ends under pinned–pinned conditions. At both supports, lateral degrees of freedom in the z-direction were constrained, while displacements along other axes were left free. The results yielded the natural frequencies along with their associated mode shapes, from which the whirling speed of the shaft was predicted.

Buckling Analysis

Buckling analysis was performed using an eigenvalue approach. One end of the shaft was fully constrained, while a unit torsional load (1 Nm) was applied at the other end. The resulting load coefficient from the eigenvalue analysis was multiplied by the applied torque to obtain the critical buckling torque. For failure prediction, the maximum strain criterion was used, assuming laminate failure occurs when shear strain reaches its limit under torsional loading. The failure index was determined. The failure index is evaluated using the following expression:

$$I_f = \frac{\varphi}{\varphi_f} \quad (1)$$

In equation 1, φ and φ_f are allowable and failure angle of twist, respectively. The angle under the torsional load at which the shaft will fail is taken as the failure angle of twist. Failure is predicted when the angle of twist reaches its ultimate limit, corresponding to a failure index of unity under the associated failure torque.

Validation of Numerical Simulation

The numerical simulation results are validated using an analytical approach. For this purpose, both solid and hollow homogeneous shafts are considered. The analytical predictions of the angle of twist, natural frequency, buckling torque, and failure index are compared with the corresponding numerical simulation results to validate the developed model. The polar moment of inertia (J) is a fundamental geometric property that characterises the torsional resistance of a circular shaft and plays a vital role in torsional analysis. For solid and hollow shafts, J is calculated using eqns.-2 and 3, respectively, where D_0 and D_i represent the outer and inner diameters of the shaft (m). The polar moment of inertia directly governs the shaft's torsional stiffness and influences the resulting angle of twist under an applied torque.[2]

$$J = \frac{\pi \times D_o^4}{32} \quad (2)$$

$$J = \frac{\pi (D_o^4 - D_i^4)}{32} \quad (3)$$

The angle of twist is expressed as follows:

$$\varphi = \frac{T \times L}{J \times G} \quad (4)$$

The natural frequency corresponding to the first mode is expressed as follows:

$$f_n = \frac{1}{2\pi}\sqrt{\frac{g\times E_x\times I}{w\times L^4}} \quad (5)$$

In eqn.-5, where the moment of inertia (I) and axial modulus (E_x) are directly related to the natural frequency (f_n). In addition, the term (g) represents the acceleration due to gravity. Weight and length of the shaft are represented by (w and L), respectively.
The buckling torque is expressed as follows:

$$T_{buckling} = 2\pi r^2 \times t \times 0.272 \times \left(E_x \times E_h^{\,3}\right)^{0.25} \times \left(\frac{t}{r}\right)^{1.5} \quad (6)$$

In eqn.-6, t represents the thickness, r is the average radius, L is the shaft length, E_x and E_h are the axial modulus and hoop modulus, respectively.

RESULTS AND DISCUSSION

Table-3 represents the comparative results of analytical equation based, numerical based and their percentage deviation.

Table-3: Comparison of Analytical and Numerical Results for Steel Shaft

Properties		Analytical Equation result (A_r)	Numerical simulation result (N_r)	Percentage deviation $\lvert A_r - N_r \rvert / A_r$ (%)
Natural frequency f_n (Hz)	SS	71.11	77.675	9.23
	HS	93.13	102.25	9.79
Angle of twist φ (°)	SS	0.228	0.23	0.877
	HS	1.5742	1.5617	0.7940
Failure index I_f	SS	0.0456	0.046	0.877
	HS	0.3148	0.3123	0.794
Buckling Torque T_b (Nm)	HS	4852.11	5312.16	9.4

*HS- Hollow shaft, SS – Solid shaft

From the comparison of analytical and numerical results as summarised in Table-3, the deviations are observed to be within 10%. Analytical and numerical results show good agreement. Natural frequencies from numerical analysis are higher by ~9–10%. Angle of twist and failure index closely match, with deviations below 1%, indicating high accuracy in torsional predictions. Buckling torque shows ~9.4% higher numerical values, likely due to improved modelling of boundary and geometric effects. Overall, analytical results are reliable for initial design, while numerical results provide more refined predictions.

Performance of Solid Shaft Versus Hollow Shaft

Solid and hollow shafts made of SM45C steel were modelled, and finite element analysis was performed to compare their torsional performance and natural frequencies. Figure-2 illustrates the comparative results for torsional strength and natural frequency between the two shaft configurations. The solid steel shaft exhibits significantly higher torsional strength (Fig.-2a), with failure torque nearly seven times that of the hollow shaft. However, this comes with a major weight penalty (~40.7 kg vs. 3.7 kg), resulting in a much lower natural frequency and poorer dynamic performance (Fig.-2b). In contrast, the hollow shaft offers ~30% higher natural frequency, lower mass, reduced vibrations, and improved critical speed. Its lower inertia also enhances vehicle acceleration and fuel efficiency. Although weaker in torsion, the hollow shaft provides a better strength-to-weight and dynamic balance, making it more suitable for high-speed automotive applications.

Effect of Fibre Orientation

A composite hollow shaft (7.23 cm diameter, 1.29 m length) made up of carbon and E-glass reinforced epoxy composite was analyzed to study the effect of fibre orientation. Fibre angle strongly influences torsional strength, natural frequency, and buckling behaviour (Fig.-3).

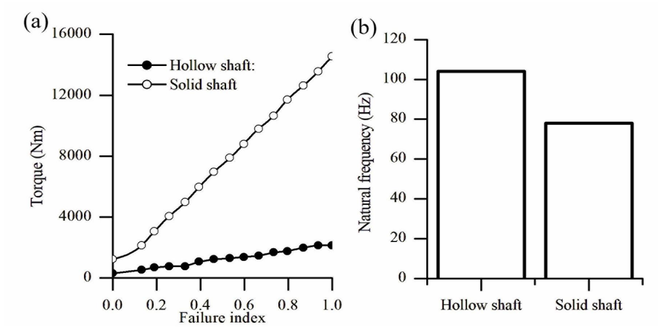

Fig.-2: Performance Comparison of Solid and Hollow Shaft

The 45° orientation provides maximum torsional strength due to effective shear load transfer, while 0° gives the minimum. In contrast, 0° yields the highest natural frequency because of maximum axial stiffness, whereas 90° results in the lowest. Buckling torque is highest at 0° and lowest at 90°, indicating its dependence on hoop stiffness (Fig.-4). Results indicate that carbon fiber epoxy composite shows superior strength and stiffness over E-glass fiber composite. The analysis demonstrates that the optimal fibre orientation varies with the performance criterion: 45° is most effective for torsional loading, whereas 0° provides superior vibration response and buckling resistance. Therefore, fiber orientation should be tailored to meet the specific design and operational requirements of the drive shaft. (Fig.-4).

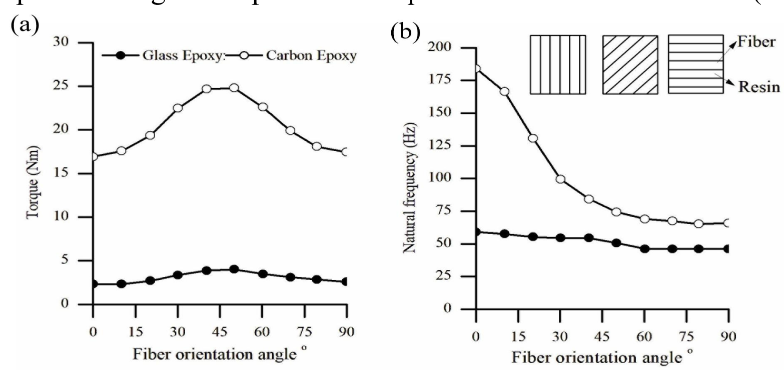

Fig.-3: Comparison of Fiber Orientation Influence on Torsional Strength and Natural Frequency In Carbon/Epoxy and E-Glass/Epoxy Laminates

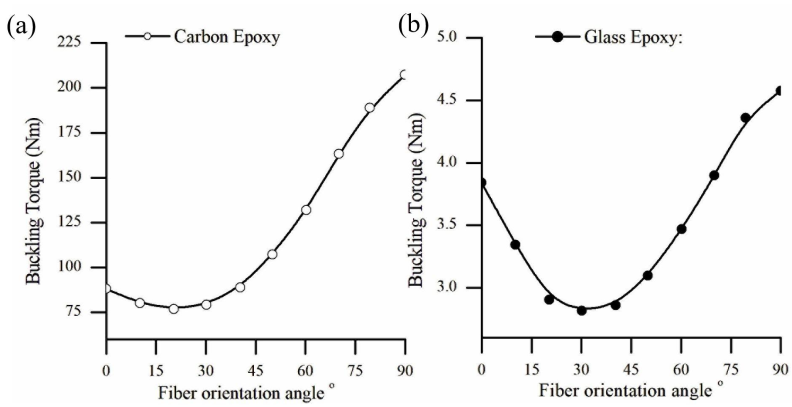

Fig.-4: Comparison of Fiber Orientation Influence on Buckling Torque in Carbon Fiber and E-Glass Fiber Epoxy Composite

Effect of Stacking Sequence

To study the influence of laminate sequence on the composite drive shaft design parameters, eight different laminate stacking configurations were taken into consideration. Of Carbon fiber © and glass fibre (G), in every instance, the shaft's geometric measurements were consistent: each shaft's length was 1.29 meters, its outside diameter was 7.23 centimetres, and its thickness was 2.0955 mm. Table-4 displays the specifics of the chosen stacking sequences. In the selected cases, the 90° and 0° plies were modelled using E-glass/epoxy laminates, while the 45° ply was chosen as carbon/epoxy.

Table-4: Different Stacking Configurations of the Composite Shaft

Case	Stacking sequence	Case	Stacking sequence
1	$0°_G/45°_C/45°_C/45°_C$	5	$90°_G/45°_C/45°_C/45°_C$
2	$45°_C/0°_G/45°_C/45°_C$	6	$45°_C/90°_G/45°_C/45°_C$
3	$45°_C/45°_C/0°_G/45°_C$	7	$45°_C/45°_C/90°_G/45°_C$
4	$45°_C/45°_C/45°_C/0°_G$	8	$45°_C/45°_C/45°_C/90°_G$

Figure-5(a) shows that placing a 45° laminate at the outermost layer significantly improves failure torque, as it effectively resists shear stresses. Configurations such as Case 5 exhibit higher torsional strength than Case 1 due to optimized ply replacement (0° with 90°), enhancing torque capacity. Natural frequency (Fig.-5(b) follows a different trend and is governed by axial stiffness; replacing 90° with 0° plies increases natural frequency (~8.3%). Although stacking sequence has a limited effect for fewer plies, its influence increases with laminate thickness. Outer 0° layers improve natural frequency but reduce torsional strength, indicating a trade-off. Buckling torque shows an inverse trend to natural frequency and increases with 90° plies due to higher hoop stiffness (Fig.-5(b)). Placing 90° laminates near the inner layers enhances buckling resistance without significantly compromising torsional performance. Overall, optimal performance requires a balanced stacking sequence: 45° outer layers for torsion, 0° for higher natural frequency, and 90° inner layers for improved buckling resistance.

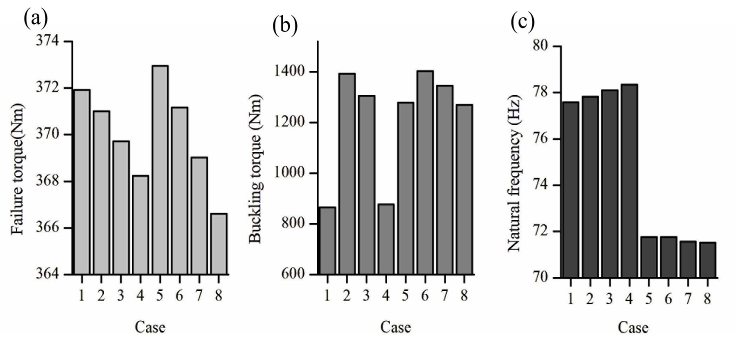

Fig.-5: Effect of Stacking Sequence on Failure Torque, Buckling Torque and Natural Frequency

Composite Drive Shaft

Following the analysis of the influence of stacking sequence on design parameters, four different composite drive shaft configurations were proposed, as summarised in Table-5. Among these, Case 12 is a Carbon/ Glass fiber reinforced hybrid composite, whereas the remaining cases are constructed entirely from carbon with epoxy plies.

Table-5: Different Configurations of the Composite Drive Shaft

Case	Laminate sequence	Number of plies	Composites
9	$[(90°)_4/(45°)_5/(0°)_2/(45°)_3]_C$	14	All carbon fibers with epoxy
10	$[(0°)_2/(90°)_3/(45°)_5/(0°)_2/(45°)_4]_C$	16	All carbon fibers with epoxy
11	$[(90°)_4/(45°)_7/(0°)_3/(45°)_3]_C$	17	All carbon fibers with epoxy
12	$[(90°)_5]_G/[(45°)_{12}/(0°)_2/(45°)_3]_C$	22	E-glass and carbon with epoxy

Figure-6 compares the torsional strength of the hollow steel shaft with different composite configurations (Cases 9–12). Torque increases nearly linearly with the failure index for all cases. Among the configurations, composite shafts consistently exhibit higher torque-carrying capacity than the hollow steel shaft. Case 12 shows the maximum torsional strength, followed by Cases 11, 10, and 9, indicating the strong influence of laminate configuration on performance. Overall, the results demonstrate that optimized composite stacking significantly enhances torsional strength compared to conventional hollow steel shafts, making them more suitable for high-performance applications. Figure-7(a) presents the comparison of natural frequency and buckling torque for composite shafts (Cases 9–12) and the hollow steel shaft. The natural frequency varies slightly among the composite cases, with Case 11 showing the highest value, while the hollow steel shaft exhibits comparable but slightly lower performance. In contrast, buckling torque (Fig.-7(b)) shows a significant improvement in composite shafts compared to the hollow steel shaft. Case 12 demonstrates the highest buckling resistance, followed by Cases 11, 10, and 9, whereas the hollow steel shaft shows substantially lower values. Overall, composite configurations provide superior buckling performance with marginal variations in natural frequency, indicating their effectiveness for lightweight and high-performance shaft applications.

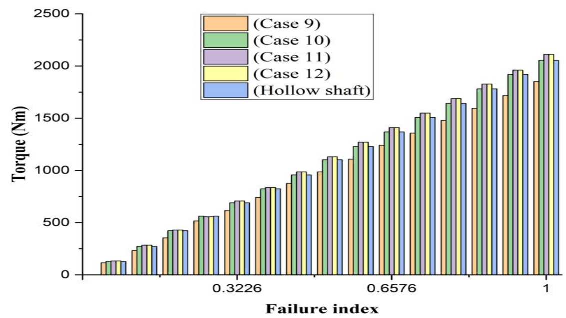

Fig.-6: Comparison of Torsional Strength of Hollow Composite and Steel Shafts

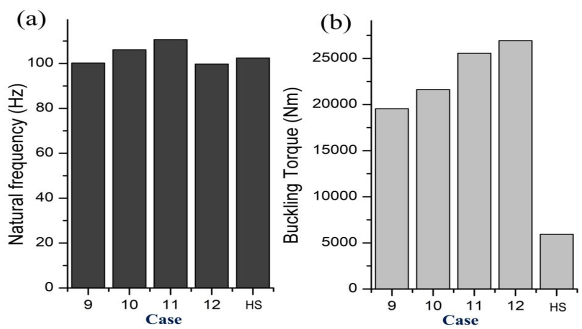

Fig.-7: Comparison of Natural Frequency and Buckling Torque of Hollow Composite and Steel Shafts

CONCLUSION

The composite drive shaft was evaluated through static stress, modal, and buckling analyses, with results validated against numerical and analytical approaches using ANSYS. The study indicates that lower fiber orientation angles increase the fundamental natural frequency due to improved bending stiffness and axial modulus. While stacking sequence has minimal influence on natural frequency in four-layer configurations, its effect becomes more significant with an increasing number of layers. Buckling torque is highly dependent on fiber orientation, reaching a maximum at 90° due to the reaching a maximum at 90° due to the high hoop-direction stiffness. Additionally, both fiber orientation and fiber laminate sequence play a significant role in determining failure torque. The placement of ±45° plies at the outer layers significantly enhances torsional strength, and increasing their proportion further improves performance, whereas the inclusion of 0° and 90° plies reduces failure torque. Furthermore, the static torque capacity is positively influenced by increasing the number of composite layers, underscoring the importance of ply configuration in optimising drive shaft design.

ACKNOWLEDGMENTS

The authors are thankful to the authorities of their institution.

CONFLICT OF INTERESTS

The authors declare that there is no conflict of interest.

AUTHOR CONTRIBUTIONS

The present work is related to *SDG-9:* Industry, Innovation and Infrastructure. All the authors contributed significantly to this manuscript, participated in reviewing/editing and approved the final draft for publication. The research profile of the authors can be verified from their ORCID ids, given below:

D. Prakash http://orcid.org/0000-0003-3503-3980
S. Martin Vinoth http://orcid.org/0000-0002-2701-9305
B. Ravi Kumar http://orcid.org/0000-0002-8696-8287

Cite this article as: D. Prakash *et al.*, *Rasayan J. Chem.*, 19(4), 1993-2000(2026), https://doi.org/10.31788/RJC.2026.1949900

REFERENCES

1. S. A. Mutasher, *Materials and Design*, **30**, 215(2009), https:// doi.org/10.1016/j.matdes.2008.05.024
2. J. Searle, M. Meng, and J. Summerscales, *Thin-Walled Structures*, **180**, 109799(2022), https://doi.org/10.1016/j.tws.2022.109799
3. B. Ravi Kumar, Ch. Naga Srimannarayana, K. Aniruth Krishnan, S.S.Hariharan, *Structural Engineering and Mechanics,* **74(4),** 515(2020), https:// doi.org/ /10.12989/sem.2020.74.4.515
4. W. Jarrett, S.P. Jeffs, F. Korkees, and M, Rawson, *Composite Structures*, **320**,117203(2023), https://doi.org/10.1016/j.compstruct.2023.117203
5. Wenzheng Zhao, Ning Pei, Chunguang Xu, *Composite Structures*, **290**, 115541(20220, https://doi.org/10.1016/j.compstruct.2022.115541
6. Mahaboob Subhani Shaik, Ravi Kumar, Hariharan Sankarasubramanian, Bonda Atchuta Ganesh Yuvaraju, *Emerging Materials Research*, **15(1)**, 21(2026), https://doi.org/10.1680/jemmr.25.00065
7. R. Singh Chahar, B. Ravi Kumar, *Steel and Composite Structures,* **31(4)**, 387(2019), https://doi.org/10.12989/scs.2019.31.4.387
8. P. Jaen-Sola, A.S. McDonald, and E. Oterkus, *Ocean Engineering*, **181**, 330(2019), https://doi.org/10.1016/j.oceaneng.2019.03.053
9. H. Zhang, S. Li, Y. Wu, P. Zhi, W. Wang, and Z. Wang, *Computer Modeling in Engineering and Sciences*, **140**, 1975(2024), https:// doi.org/10.32604/cmes.2024.050185
10. A. N. Halilbeşe, *Journal of Naval Architecture and Marine Technology,* **227(1)**, 43(2025), https://doi.org/ 10.54926/jnamt.2025.248
11. T. C. Henry, and B. T. Mills, *Composite Structures*, **207**, 438(2019), https://doi.org/10.1016/j.compstruct.2018.09.049
12. Badie, M. A., Mahdi, E., and Hamouda, A. M. S., *Materials and Design*, **32**,1485(2011), https://doi.org/10.1016/j.matdes.2010.08.042
13. B. F. Morales-Hernández, H. G. Sánchez-Acevedo, and R. G. Barrera-Santos, *The International Journal of Advanced Manufacturing Technology*, **139,** 1581(2025), https:// doi.org/10.1007/s00170-025-15863-7
14. H. B. H. Gubran, *Mechanics Research Communications*, **32,** 368(2005), https://doi.org/10.1016/j.mechrescom.2005.02.005
15. T. S. Kalaskar, K. H. Munde, and A. R. Pawar, *Journal of Analysis and Computation*, **15**, 27(2021), https:// doi.org/ 10.21203/rs.3.rs-7777720/v1
16. H. S. Kim, J. W. Kim, and J. K. Kim, *Composite structures*, **63**, 87(2004), https://doi.org/10.1016/S0263-8223(03)00136-3
17. S. S. Nadeem, G. Giridhara, and H. K. Rangavittal, *Materials Today: Proceedings*, **5**, 2738(2018), https://doi.org/10.1016/j.matpr.2018.01.058
18. Y. Hu, M. Yang, J. Zhang, C. Song, and T. Hong, *Advanced Composite Materials*, **26,** 537(2017), https://doi.org/10.1080/09243046.2016.1207126
19. Y. A. Khalid, S. A. Mutasher, B. B. Sahari, and A. M. S. Hamouda, *Materials and Design*, **28**, 329(2007), https://doi.org/10.1016/j.matdes.2005.05.021

[RJC-9900/2026]